ACS Photonics

Article

pubs.acs.org/journal/apchd5

Dual-Band Light Focusing Using Stacked Graphene Metasurfaces

Wei Ma,[†] Zhong Huang,[†,‡] Xiaokang Bai,[†] Peng Zhan,[‡] and Yongmin Liu*[,†,§]

[†]Department of Mechanical and Industrial Engineering and [§]Department of Electrical and Computer Engineering, Northeastern University, Boston, Massachusetts 02115, United States

[‡]School of Physics and National Laboratory of Solid State Microstructures, Nanjing University, Nanjing 210093, China

ABSTRACT: In this article, we theoretically study the optical properties of graphene metasurfaces consisting of layered graphene ribbons and their potential applications as multifunctional optical devices in the long-wavelength infrared region. By engineering the plasmonic resonance in graphene ribbons with different widths, the phase of reflected light can be tuned over a range of nearly 2π, while the reflectivity is kept relatively high at the target frequencies. Owing to the weak light−graphene interaction in the off-resonance region, independent control of the reflected light can be achieved by stacking multiple layers of graphene ribbons. Since the interlayer coupling between the ribbons is negligible, we have developed a transmission-line-based uncoupled model as a physical interpretation of the stacked metasurface. The modeled results show excellent agreement with numerical simulations. As a proof-of-principle demonstration, we have designed and demonstrated graphene metasurfaces as flat, dual-band focusing reflectors operating at 25 and 16 THz. Our work provides a general design scheme for multiband, multifunctional metasurfaces with various potential applications, including beam steering, optical communication, and information processing.

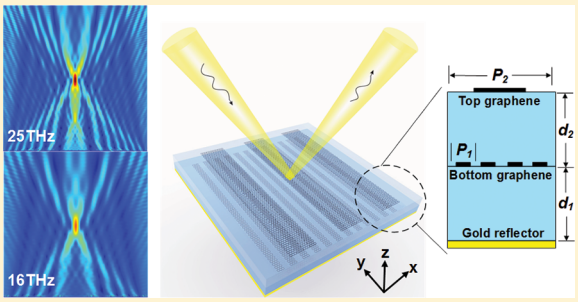

KEYWORDS: *graphene, metasurface, multifunctional, infrared*

Metamaterials are artificial materials composed of rationally designed subwavelength structures with exotic properties unavailable in nature.[1−3] As the two-dimensional equivalents of metamaterials, metasurfaces can enforce abrupt changes on the phase, amplitude, or polarization of light, by designing the geometry of the constituent subwavelength building blocks and their spatial arrangement.[4−7] On the basis of the modulation of optical properties of metasurfaces, various optical functionalities have been demonstrated, such as focusing,[8,9] gradient index diffraction grating,[10] wave plates,[11] beam deflection,[12,13] and holograms.[14] In most cases, the spectral responses of such planar optical devices were achieved by engineering either plasmonic resonances in metallic structures or Mie resonances in high-index dielectric structures.[15−17]

Graphene, as a two-dimensional material consisting of a monolayer of carbon atoms,[18] has attracted extensive interest in the design of infrared plasmonic structures, metamaterials, and metasurfaces due to its unique optical and electronic properties.[19−22] The Fermi level and therefore the surface conductivity of graphene can be easily tuned by chemical doping or electrical gating,[23] which is a prominent advantage over the conventional metals. Due to the intrinsically weak interaction between light and monolayer graphene, a variety of novel metamaterials and plasmonic devices have been proposed and demonstrated by using either patterned graphene[24−33] or hybrid graphene−metal composites[34−39] to enhance the interaction for spectrally tunable applications. However, despite the strong field enhancement, the nature of the resonance also renders the response of such devices usually narrow-band. In order to achieve broadband or multiband performance for metasurfaces, a common solution is to employ a planar multiplexed design by combining different sets of resonators operating at different target frequencies.[40−42] Particularly for graphene metasurfaces, apart from changing their geometries, the Fermi level of each individual resonator can be tuned separately to respond to different frequencies.[43,44] Apparently, a major drawback of this planar configuration is its low efficiency, because each working frequency or functionality essentially comes from the contribution of only a portion of the metasurface area. Moreover, individually tuning the Fermi level in the graphene metasurface is not a very practical experimental approach, since the constituent resonators are deep subwavelength in dimension, which is determined by the highly confined surface plasmon at the graphene−dielectric interface.[45]

In this article, taking advantage of the otherwise undesired weak interaction between light and graphene at the off-resonance condition, we propose a feasible and efficient solution to implementing multiband metasurfaces based on a stacked graphene configuration. As a proof-of-concept demonstration, dual-band focusing reflectors using stacked graphene ribbon arrays are designed and numerically verified, with the focusing points either along or away from the device symmetry axis at two distinct working frequencies of 16 and 25 THz,

Received: April 3, 2017
Published: June 7, 2017

DOI: 10.1021/acsphotonics.7b00351
ACS Photonics 2017, 4, 1770−1775

respectively. To clarify the underlying physics of the stacked structure, we apply a transmission-line-based uncoupled model, in which the graphene ribbon is described by its effective surface conductivity. The excellent agreement between the modeling and simulation results provides a general design guideline for multiband and multifunctional graphene metasurfaces.

RESULTS AND DISCUSSION

The structure of the proposed dual-band focusing reflector is schematically shown in Figure 1a. It consists of an optically thick gold layer at the bottom serving as a perfect reflector to eliminate transmission. Four alternating layers of dielectric and graphene ribbons are stacked sequentially on top of a gold reflector. The two dielectric layers are assumed to be infrared transparent materials (e.g., CaF_2 and MgF_2) with a refractive index of 1.4. The dielectric spacer together with the back reflector forms as an optical cavity to enhance the light–graphene interaction. The reflected phase and amplitude periodically vary with the spacer thickness.[30] The two dielectric layers are optimized to have the same thickness of 2 μm, which ensures a phase modulation of almost 2π while maintaining high reflectivity at the target wavelengths. The inset of Figure 1a shows the cross-sectional view of a unit cell of the metasurface. The period of the bottom graphene ribbon array is P_1 = 0.25 μm, while the period of the top graphene ribbon array is P_2 = 1 μm. Therefore, the composite unit cell of the metasurface contains one unit of top ribbons and four units of bottom ribbons. By varying the width of the ribbons in either the top or bottom layer independently, the phase of the reflected light can be tuned separately at two distinct frequencies.

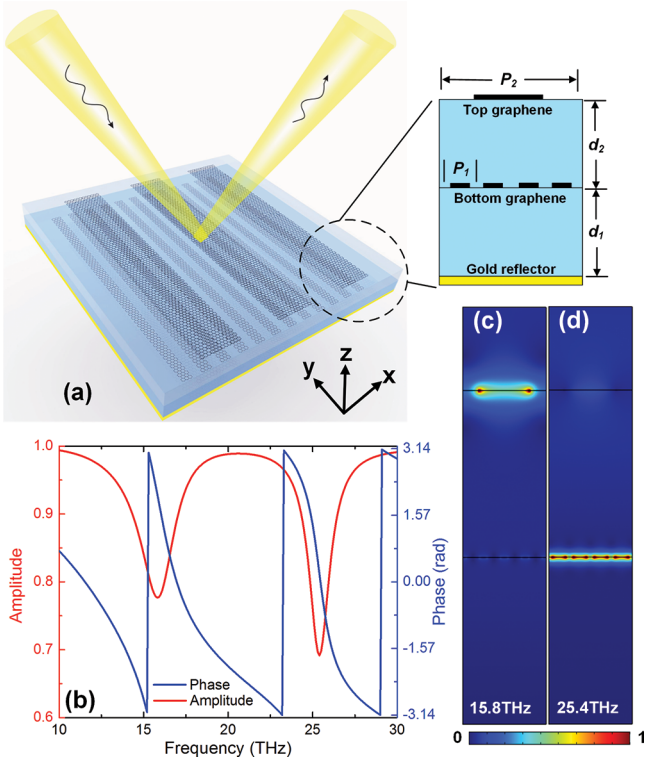

Figure 1. (a) Schematic of the proposed dual-band focusing reflector. The thicknesses of the two dielectric spacers (d_1 and d_2) are both 2 μm. The periods of the bottom graphene ribbons and top graphene ribbons are P_1 = 0.25 μm and P_2 = 1 μm, respectively. (b) Spectral response of a unit cell with a top ribbon width of 600 nm and bottom ribbon width of 160 nm. The red and blue curves correspond to the amplitude and phase of the reflected wave, respectively. The relative magnitude of electric fields at two resonant frequencies of (c) 15.8 THz and (d) 25.4 THz, respectively.

In order to verify the dual-band phase tuning ability of the proposed stacked graphene metasurface, the spectral response of a single unit cell is first investigated, where the top ribbon width and bottom ribbon width are fixed at 600 and 160 nm, respectively. As shown in Figure 1b, two resonant dips are observed at 15.8 and 25.4 THz accompanied with a phase change of almost 2π around the resonant frequencies. To better illustrate the origin of these two resonances, the normalized magnitudes of the electric field distribution are plotted at the two resonant frequencies. At 15.8 THz, the field mainly concentrates around the top graphene ribbons with a larger width, while the near field is barely enhanced around the narrower ribbons at the bottom (Figure 1c). In contrast, at the higher resonant frequency of 25.4 THz, the electric field is strongly localized near the bottom graphene ribbons (Figure 1d).

Due to graphene's two-dimensional nature with a monolayer of carbon atoms, the interaction between light and graphene is very weak, which is usually a drawback to be overcome in most optoelectronic devices.[45] Here, however, this feature is utilized instead in designing the stacked graphene metasurfaces. At one of the resonant frequencies, the corresponding graphene ribbon layer is functioning, while for the other layer, the light–graphene interaction is fairly weak, making it almost transparent. Therefore, the two layers of graphene ribbons can be adjusted independently in response to different target wavelengths without mutual interference with each other. This is practically difficult by using stacked metallic structures.

To have a clear physical insight into the proposed stacked graphene metasurface, we have established an uncoupled model based on the transmission line theory. As shown in Figure 2a, the metasurface can be decoupled into a system with three

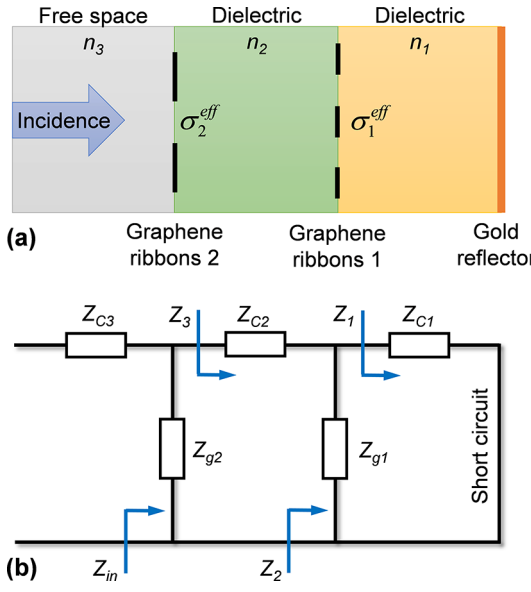

Figure 2. (a) Proposed metasurface as an uncoupled system. (b) Transmission line model for the proposed metasurface with graphene ribbons described by lumped impedances.

DOI: 10.1021/acsphotonics.7b00351
ACS Photonics 2017, 4, 1770–1775

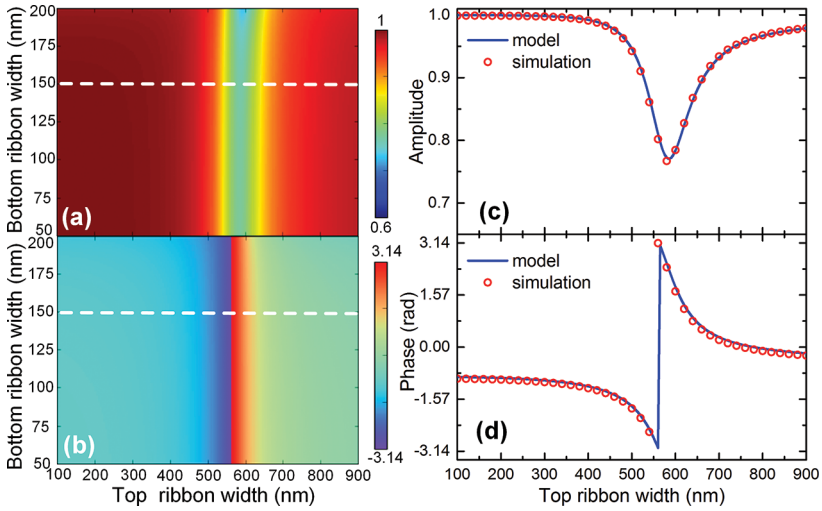

Figure 3. Optical response of the proposed dual-band metasurface at the working frequency of 16 THz. Reflection amplitude (a) and phase (b) map of the metasurface when changing the bottom ribbon width from 50 nm to 200 nm and the top ribbon width from 100 nm to 900 nm. Variation of amplitude (c) and phase (d) when changing the top ribbon width from 100 nm to 900 nm while keeping the bottom ribbon width constant at 150 nm (indicated by the dashed lines in the left plots). The blue curve is obtained from the transmission line model, and the red hollow circles are numerically simulated results by COMSOL Multiphysics.

interfaces and three dielectric media. The gold reflector at the bottom is treated as a perfect electric conductor (PEC), a good approximation for metals at long-wavelength infrared frequencies, while the two layers of graphene ribbons are described by their effective surface conductivities (σ_1^{eff} and σ_2^{eff}). The two dielectric spacers (n_1 and n_2) and free space (n_3) are characterized by their corresponding refractive indices. By eliminating the interlayer coupling between the graphene layers, the entire device can be modeled as an equivalent transmission line with parallel lumped elements, as illustrated in Figure 2b. The bottom PEC layer corresponds to a short circuit at one end, while each dielectric layer is modeled by cascaded transmission lines with specific characteristic impedances determined by their refractive indices. The two-dimensional graphene ribbons are represented as lumped impedances (Z_{g1} and Z_{g2}) at the connecting points between different transmission lines.

Since the effective surface conductivity (σ^{eff}) of graphene ribbons is difficult to obtain directly, we retrieved it from the numerically calculated transmission spectrum as[46]

$$\sigma^{\text{eff}} = 2/t - (1 + n_t/n_i) \tag{1}$$

where t represents the transmission coefficient of light through graphene ribbons that are sandwiched between two semi-infinite dielectric layers. Light is incident from one dielectric medium with refractive index n_i, passes through graphene ribbons, and transmits to a second medium with refractive index n_t sequentially. The transmission coefficient is dependent on all the graphene ribbon properties such as the width, chemical potential, and mobility, which are incorporated in the numerical simulations. The lumped impedance is simply the reciprocal of the effective surface conductivity of graphene ribbons. The overall input impedance in the transmission line model can thus be calculated level by level, as indicated in Figure 2b. Starting from the short-circuit end, zero impedance is transformed to Z_1 along the bottom 2 μm long transmission line, which is then in parallel with the bottom graphene impedance Z_{g1} and becomes Z_2. Next, Z_2 is transformed along the top transmission line, and the impedance Z_3 is parallel to the top graphene impedance Z_{g2}, which becomes the input impedance of the entire two-layer system (Z_{in}). The overall reflection coefficient (r) from the metasurface is given by

$$r = (Z_{in} - Z_{c3})/(Z_{in} + Z_{c3}) \tag{2}$$

where Z_{c3} = 377 Ω is the impedance of the free space in our case.

With eq 2, the performance of the metasurface unit cell can be systematically yet very efficiently investigated by varying its geometric parameters. Figure 3 demonstrates the performance of the unit cell at the working frequency of 16 THz, where the top graphene ribbons with larger dimension play a dominant role. As illustrated in the analytical results in Figure 3a and b based on the transmission line model, the reflection coefficients are almost independent of the width of the bottom graphene ribbons at 16 THz, which is consistent with the simulation prediction in Figure 1b. However, when changing the width of the top graphene ribbons from 100 to 900 nm, the reflection coefficients exhibit an evident resonance behavior, with a dip in amplitude accompanied by a phase change of nearly 2π around the ribbon width of 600 nm. The relatively high reflection amplitude and the full 2π phase control are essential to the complete and efficient manipulation of the reflected wave by metasurfaces. Figure 3c and d plot the modeled reflection coefficients for various widths of the top graphene ribbons with a fixed bottom ribbon width of 150 nm (indicated by the white dashed lines in the corresponding maps on the left). For comparison, the full-wave simulation results are marked as red circles in the same plots, which agree perfectly with the calculation from the transmission line model. Such a perfect agreement is evidence for the negligible interlayer coupling among the graphene ribbons, in contrast to their metallic counterpart, where a similar decoupled model produces more discrepancy from the simulation.[47] The interlayer coupling between graphene ribbons mainly depends on the penetration depth of graphene surface plasmons into the dielectric layer. Owing to the intensely localized surface plasmon at the graphene−dielectric interface with a strong confinement factor more than 10 times larger than that of a metal, the coupling

DOI: 10.1021/acsphotonics.7b00351
ACS Photonics 2017, 4, 1770−1775

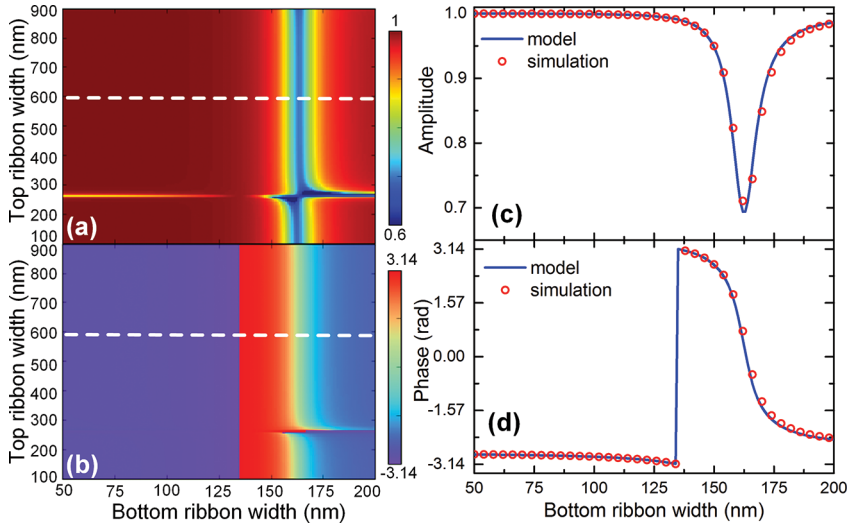

Figure 4. Optical response of the proposed dual-band metasurface at the working frequency of 25 THz. Reflection amplitude (a) and phase (b) map of the metasurface when changing the bottom ribbon width from 50 to 200 nm and the top ribbon width from 100 to 900 nm. Variation of amplitude (c) and phase (d) when changing the bottom ribbon width from 50 nm to 200 nm while keeping the top ribbon width constant at 600 nm (indicated by the dashed lines in the left plots). The blue curve is obtained from the transmission line model, and the red hollow circles are numerically simulated results by COMSOL Multiphysics.

between the two layers of graphene ribbons can be neglected,[45] and the functionalities of the two-layer graphene ribbons can be tuned separately. In fact, according to our simulations, the shift of spectra due to interlayer coupling becomes observable only when the spacer thickness is below 200 nm, which is 10 times smaller than the value in the current design.

The performance of the unit cell at 25 THz is depicted in Figure 4, which depends almost only on the bottom graphene ribbons. The distortion in the reflection maps (Figure 4a and b) is caused by the high-order resonance induced in the top graphene ribbon when its width is around 250 nm. Apart from this narrow distortion, the overall optical response is similar to that at 16 THz. By varying the widths of the bottom graphene ribbons, the plasmonic resonance can be harnessed to achieve a phase change of nearly 2π while maintaining a high reflectivity. When the top ribbon width is fixed at 600 nm, the comparison in reflection coefficients between modeled results and simulated results also gives excellent consistency (Figure 4c and d).

As a proof-of-concept demonstration of the proposed stacked graphene configuration, we have designed two metasurface focusing reflectors working at 16 and 25 THz simultaneously. The two-dimensional focusing reflector requires a hyperbolic phase profile given by

$$\Delta\varphi(x) = \frac{2\pi}{\lambda}\left(\sqrt{(x-\Delta x)^2 + f^2} - f\right) \tag{3}$$

where f is the designed focal length, Δx is the horizontal offset of the focal point from the center, and λ is the wavelength in free space.

The parabolic reflector is a widely used optical component in energy harvesting and imaging applications, which can focus normally incident light along its symmetry axis at certain points. We first design a dual-band, planar version of the parabolic reflector working at both 25 and 16 THz. Following the relationship in eq 3 with $\Delta x = 0$, the metasurface is designed with a lateral dimension of 400 μm and the same focal length f = 200 μm for both working frequencies. With the target phase shifts determined by eq 3, the corresponding widths of the ribbons at the top and bottom layers are obtained directly from Figure 3 and Figure 4. The overall performance of the device was evaluated by full-wave simulations using plane wave illumination with an electric field amplitude of 1 V/m at normal incidence. As shown in Figure 5, a strong focusing effect

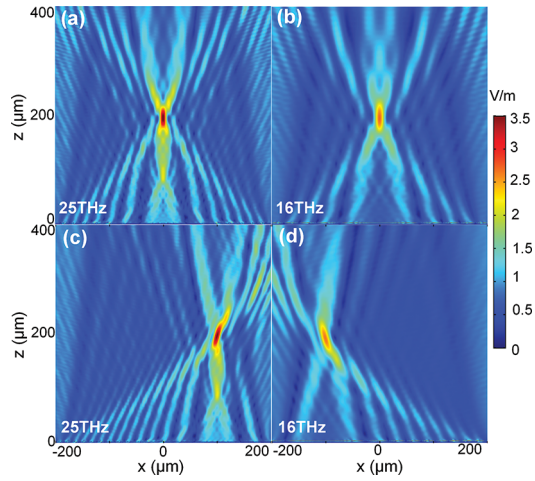

Figure 5. Simulated electric field distribution, which shows the performance of the dual-band focusing reflector based on stacked graphene metasurfaces under plane wave illumination at normal incidence. Parabolic reflector at the working frequency of 25 THz (a) and 16 THz (b). Off-axis focusing reflector at the working frequency of 25 THz (c) and 16 THz (d). For clarity, only the reflected light is plotted in all the figures.

is observed at the designed focal length for both 25 and 16 THz, where the incident light is subtracted in the field map for clarity. Due to the shorter wavelength, the focal point is smaller with higher intensity for 25 THz incidence than that for 16 THz. For potential experimental verification, the focusing effect can be measured by either tilting the incident light by a small angle from the normal direction[48] or employing another optical component such as a beam splitter to differentiate incident and reflected light.[49]

DOI: 10.1021/acsphotonics.7b00351
ACS Photonics 2017, 4, 1770−1775

Besides the common parabolic reflector, the stacked graphene configuration also allows us to individually design the focusing properties for the target frequencies. To this end, another focusing reflector is designed, which focuses the normally incident light at two different off-axis positions at 25 and 16 THz. Such a device is useful in various applications, including wavelength division multiplexing or frequency-distinguishable infrared detection. In our case, with the offset distance $\Delta x = 100\ \mu$m for 25 THz and $\Delta x = -100\ \mu$m for 16 THz, the calculated phase profile is imposed on the top graphene ribbon and bottom graphene ribbons, respectively. The full-wave simulation results are depicted in Figure 5c and d, showing the separation of the focal points at the two target frequencies, where the same focal length is achieved with the corresponding designed offsets.

In conclusion, we have systematically studied the spectral responses of stacked graphene ribbons and demonstrated a practical and efficient implementation of dual-band focusing reflectors based on this configuration. The highly confined surface plasmon around graphene and thus very weak coupling between different layers are fully utilized, with which different dimensions of graphene ribbons can be independently designed for the two distinct working frequencies of 25 and 16 THz, respectively. Moreover, the dual-band functionality can be well explained by a transmission-line-based uncoupled model, in excellent agreement with numerical simulations. It should be emphasized that the proposed stacked configuration provides a general platform for multiband and multifunctional graphene metasurfaces. More functions could be incorporated by stacking more layers or even in combination with planar multiplexed arrangements. The inherent tunable optical properties of graphene by electrical or chemical doping can also be readily exploited in the proposed design, such as individually tuning the chemical potential of the ribbons for broadband response[43] or simultaneously tuning the entire layer for on−off switching.[30] The versatility of the stacked graphene metasurface manifests a broad range of potential applications in tunable, lightweight, and integrated optoelectronic systems.

METHODS

The commercial finite element package COMSOL Multiphysics is used to calculate the electromagnetic response from graphene ribbon arrays. The electromagnetic wave module is used with a frequency domain solver. The simulations are performed on a 2D structure, where the graphene ribbons are assumed to be infinitely long. In the simulation, graphene was characterized by its surface conductivity using the Kubo formula,[50] and the Fermi energy of graphene around 0.64 eV and the mobility of 10 000 $cm^2/(V\ s)$ was assumed.[51] The bottom reflector is treated as a PEC, while the dielectric spacer is modeled as a lossless dielectric with a refractive index of 1.4.

AUTHOR INFORMATION

Corresponding Author

*E-mail: y.liu@northeastern.edu.

ORCID

Yongmin Liu: 0000-0003-1084-6651

Notes

The authors declare no competing financial interest.

ACKNOWLEDGMENTS

Y.L. acknowledges the support of the Office of Naval Research (N00014-16-1-2409) and the 3M Non-Tenured Faculty Award. P.Z. acknowledges the support of the National Natural Science Foundation of China under grant number 11674166.

REFERENCES

(1) Shelby, R. A.; Smith, D. R.; Schultz, S. Experimental verification of a negative index of refraction. *Science* **2001**, *292*, 77−79.

(2) Liu, Y.; Zhang, X. Metamaterials: a new frontier of science and technology. *Chem. Soc. Rev.* **2011**, *40*, 2494−2507.

(3) Soukoulis, C. M.; Wegener, M. Past achievements and future challenges in the development of three-dimensional photonic metamaterials. *Nat. Photonics* **2011**, *5*, 523−530.

(4) Yu, N.; Genevet, P.; Kats, M. A.; Aieta, F.; Tetienne, J.-P.; Capasso, F.; Gaburro, Z. Light propagation with phase discontinuities: generalized laws of reflection and refraction. *Science* **2011**, *334*, 333−337.

(5) Holloway, C. L.; Kuester, E. F.; Gordon, J. A.; O'Hara, J.; Booth, J.; Smith, D. R. An overview of the theory and applications of metasurfaces: The two-dimensional equivalents of metamaterials. *IEEE Antenn. Propag. M.* **2012**, *54*, 10−35.

(6) Kildishev, A. V.; Boltasseva, A.; Shalaev, V. M. Planar photonics with metasurfaces. *Science* **2013**, *339*, 1232009.

(7) Yu, N.; Capasso, F. Flat optics with designer metasurfaces. *Nat. Mater.* **2014**, *13*, 139−150.

(8) Aieta, F.; Genevet, P.; Kats, M. A.; Yu, N.; Blanchard, R.; Gaburro, Z.; Capasso, F. Aberration-free ultrathin flat lenses and axicons at telecom wavelengths based on plasmonic metasurfaces. *Nano Lett.* **2012**, *12*, 4932−4936.

(9) Yang, Q.; Gu, J.; Wang, D.; Zhang, X.; Tian, Z.; Ouyang, C.; Singh, R.; Han, J.; Zhang, W. Efficient flat metasurface lens for terahertz imaging. *Opt. Express* **2014**, *22*, 25931−25939.

(10) Tsai, Y.-J.; Larouche, S.; Tyler, T.; Lipworth, G.; Jokerst, N. M.; Smith, D. R. Design and fabrication of a metamaterial gradient index diffraction grating at infrared wavelengths. *Opt. Express* **2011**, *19*, 24411−24423.

(11) Pors, A.; Bozhevolnyi, S. I. Efficient and broadband quarter-wave plates by gap-plasmon resonators. *Opt. Express* **2013**, *21*, 2942−2952.

(12) Pfeiffer, C.; Emani, N. K.; Shaltout, A. M.; Boltasseva, A.; Shalaev, V. M.; Grbic, A. Efficient light bending with isotropic metamaterial huygens' surfaces. *Nano Lett.* **2014**, *14*, 2491−2497.

(13) Neu, J.; Beigang, R.; Rahm, M. Metamaterial-based gradient index beam steerers for terahertz radiation. *Appl. Phys. Lett.* **2013**, *103*, 041109.

(14) Zheng, G.; Mühlenbernd, H.; Kenney, M.; Li, G.; Zentgraf, T.; Zhang, S. Metasurface holograms reaching 80% efficiency. *Nat. Nanotechnol.* **2015**, *10*, 308−312.

(15) Genevet, P.; Capasso, F.; Aieta, F.; Khorasaninejad, M.; Devlin, R. Recent advances in planar optics: from plasmonic to dielectric metasurfaces. *Optica* **2017**, *4* (1), 139−152.

(16) Lin, D.; Fan, P.; Hasman, E.; Brongersma, M. L. Dielectric gradient metasurface optical elements. *Science* **2014**, *345*, 298−302.

(17) Moitra, P.; Slovick, B. A.; Yu, Z. G.; Krishnamurthy, S.; Valentine, J. Experimental demonstration of a broadband all-dielectric metamaterial perfect reflector. *Appl. Phys. Lett.* **2014**, *104*, 171102.

(18) Geim, A. K.; Novoselov, K. S. The rise of graphene. *Nat. Mater.* **2007**, *6*, 183−191.

(19) Koppens, F. H.; Chang, D. E.; Garcia de Abajo, F. J. Graphene plasmonics: a platform for strong light−matter interactions. *Nano Lett.* **2011**, *11*, 3370−3377.

(20) Bao, Q.; Loh, K. P. Graphene photonics, plasmonics, and broadband optoelectronic devices. *ACS Nano* **2012**, *6*, 3677−3694.

(21) Chen, J.; Badioli, M.; Alonso-González, P.; Thongrattanasiri, S.; Huth, F.; Osmond, J.; Spasenović, M.; Centeno, A.; Pesquera, A.; Godignon, P. Optical nano-imaging of gate-tunable graphene plasmons. *Nature* **2012**, *487*, 77−81.

DOI: 10.1021/acsphotonics.7b00351
ACS Photonics 2017, 4, 1770−1775

(22) Fei, Z.; Rodin, A.; Andreev, G.; Bao, W.; McLeod, A.; Wagner, M.; Zhang, L.; Zhao, Z.; Thiemens, M.; Dominguez, G. Gate-tuning of graphene plasmons revealed by infrared nano-imaging. *Nature* **2012**, *487*, 82−85.
(23) Neto, A. C.; Guinea, F.; Peres, N. M.; Novoselov, K. S.; Geim, A. K. The electronic properties of graphene. *Rev. Mod. Phys.* **2009**, *81*, 109.
(24) Yao, G.; Ling, F.; Yue, J.; Luo, C.; Ji, J.; Yao, J. Dual-band tunable perfect metamaterial absorber in the THz range. *Opt. Express* **2016**, *24*, 1518−1527.
(25) Yang, C.; Luo, Y.; Guo, J.; Pu, Y.; He, D.; Jiang, Y.; Xu, J.; Liu, Z. Wideband tunable mid-infrared cross polarization converter using rectangle-shape perforated graphene. *Opt. Express* **2016**, *24*, 16913−16922.
(26) Zhang, Y.; Feng, Y.; Zhu, B.; Zhao, J.; Jiang, T. Switchable quarter-wave plate with graphene based metamaterial for broadband terahertz wave manipulation. *Opt. Express* **2015**, *23*, 27230−27239.
(27) He, X. Tunable terahertz graphene metamaterials. *Carbon* **2015**, *82*, 229−237.
(28) Fan, Y.; Shen, N.-H.; Koschny, T.; Soukoulis, C. M. Tunable terahertz meta-surface with graphene cut-wires. *ACS Photonics* **2015**, *2*, 151−156.
(29) Fang, Z.; Wang, Y.; Schlather, A. E.; Liu, Z.; Ajayan, P. M.; García de Abajo, F. J.; Nordlander, P.; Zhu, X.; Halas, N. J. Active tunable absorption enhancement with graphene nanodisk arrays. *Nano Lett.* **2013**, *14*, 299−304.
(30) Li, Z.; Yao, K.; Xia, F.; Shen, S.; Tian, J.; Liu, Y. Graphene plasmonic metasurfaces to steer infrared light. *Sci. Rep.* **2015**, *5*, 12423.
(31) Ju, L.; Geng, B.; Horng, J.; Girit, C.; Martin, M.; Hao, Z.; Bechtel, H. A.; Liang, X.; Zettl, A.; Shen, Y. R. Graphene plasmonics for tunable terahertz metamaterials. *Nat. Nanotechnol.* **2011**, *6*, 630−634.
(32) Yan, H.; Li, X.; Chandra, B.; Tulevski, G.; Wu, Y.; Freitag, M.; Zhu, W.; Avouris, P.; Xia, F. Tunable infrared plasmonic devices using graphene/insulator stacks. *Nat. Nanotechnol.* **2012**, *7*, 330−334.
(33) Gomez-Diaz, J.; Tymchenko, M.; Alù, A. Hyperbolic metasurfaces: surface plasmons, light-matter interactions, and physical implementation using graphene strips [Invited]. *Opt. Mater. Express* **2015**, *5*, 2313−2329.
(34) Kim, S.; Jang, M. S.; Brar, V. W.; Tolstova, Y.; Mauser, K. W.; Atwater, H. A. Electronically tunable extraordinary optical transmission in graphene plasmonic ribbons coupled to subwavelength metallic slit arrays. *Nat. Commun.* **2016**, *7*, 12323.
(35) Dabidian, N.; Dutta Gupta, S.; Kholmanov, I.; Lai, K.; Lu, F.; Lee, J.; Jin, M.; Trendafilov, S.; Khanikaev, A.; Fallahazad, B. Experimental Demonstration of Phase Modulation and Motion Sensing Using Graphene-Integrated Metasurfaces. *Nano Lett.* **2016**, *16*, 3607−3615.
(36) Zhang, Y.; Li, T.; Chen, Q.; Zhang, H.; O'Hara, J. F.; Abele, E.; Taylor, A. J.; Chen, H.-T.; Azad, A. K. Independently tunable dual-band perfect absorber based on graphene at mid-infrared frequencies. *Sci. Rep.* **2016**, *5*, 18463.
(37) Yao, Y.; Shankar, R.; Kats, M. A.; Song, Y.; Kong, J.; Loncar, M.; Capasso, F. Electrically tunable metasurface perfect absorbers for ultrathin mid-infrared optical modulators. *Nano Lett.* **2014**, *14*, 6526−6532.
(38) Emani, N. K.; Chung, T.-F.; Kildishev, A. V.; Shalaev, V. M.; Chen, Y. P.; Boltasseva, A. Electrical modulation of Fano resonance in plasmonic nanostructures using graphene. *Nano Lett.* **2013**, *14*, 78−82.
(39) Lee, S. H.; Choi, M.; Kim, T.-T.; Lee, S.; Liu, M.; Yin, X.; Choi, H. K.; Lee, S. S.; Choi, C.-G.; Choi, S.-Y. Switching terahertz waves with gate-controlled active graphene metamaterials. *Nat. Mater.* **2012**, *11*, 936−941.
(40) Hu, J.; Liu, C.-H.; Ren, X.; Lauhon, L. J.; Odom, T. W. Plasmonic Lattice Lenses for Multiwavelength Achromatic Focusing. *ACS Nano* **2016**, *10*, 10275−10282.
(41) Maguid, E.; Yulevich, I.; Veksler, D.; Kleiner, V.; Brongersma, M. L.; Hasman, E. Photonic spin-controlled multifunctional shared-aperture antenna array. *Science* **2016**, *352*, 1202−1206.
(42) Ma, W.; Wen, Y.; Yu, X. Broadband metamaterial absorber at mid-infrared using multiplexed cross resonators. *Opt. Express* **2013**, *21*, 30724−30730.
(43) Liu, L.; Zarate, Y.; Hattori, H. T.; Neshev, D. N.; Shadrivov, I. V.; Powell, D. A. Terahertz focusing of multiple wavelengths by graphene metasurfaces. *Appl. Phys. Lett.* **2016**, *108*, 031106.
(44) Lu, F.; Liu, B.; Shen, S. Infrared Wavefront Control Based on Graphene Metasurfaces. *Adv. Opt. Mater.* **2014**, *2*, 794−799.
(45) Low, T.; Avouris, P. Graphene plasmonics for terahertz to mid-infrared applications. *ACS Nano* **2014**, *8*, 1086−1101.
(46) Andryieuski, A.; Lavrinenko, A. V. Graphene metamaterials based tunable terahertz absorber: effective surface conductivity approach. *Opt. Express* **2013**, *21*, 9144−9155.
(47) Chen, H.-T. Interference theory of metamaterial perfect absorbers. *Opt. Express* **2012**, *20*, 7165−7172.
(48) Ma, W.; Jia, D.; Yu, X.; Feng, Y.; Zhao, Y. Reflective gradient metasurfaces for polarization-independent light focusing at normal or oblique incidence. *Appl. Phys. Lett.* **2016**, *108*, 071111.
(49) Pors, A.; Nielsen, M. G.; Eriksen, R. L.; Bozhevolnyi, S. I. Broadband focusing flat mirrors based on plasmonic gradient metasurfaces. *Nano Lett.* **2013**, *13*, 829−834.
(50) Hanson, G. W. Dyadic Green's functions and guided surface waves for a surface conductivity model of graphene. *J. Appl. Phys.* **2008**, *103*, 064302.
(51) Jablan, M.; Buljan, H.; Soljačić, M. Plasmonics in graphene at infrared frequencies. *Phys. Rev. B: Condens. Matter Mater. Phys.* **2009**, *80*, 245435.

DOI: 10.1021/acsphotonics.7b00351
ACS Photonics 2017, 4, 1770−1775